

Probing maximal flavor changing Z' in $U(1)_{L_\mu-L_\tau}$ at μ TRISTAN

Fei Huang^{1*} and Jin Sun^{2†}

¹*School of Physics and Technology, University of Jinan, Jinan, Shandong 250022, China and*

²*Particle Theory and Cosmology Group, Center for Theoretical Physics of the Universe, Institute for Basic Science (IBS), Daejeon 34126, Korea*

We explore the potential to detect the $U(1)_{L_\mu-L_\tau}$ model featuring triplet scalars Δ at the μ TRISTAN collider. The new gauge boson Z' , arising from the spontaneous breaking of $U(1)_{L_\mu-L_\tau}$, can exhibit maximal flavor changing interactions under the exchange symmetry, while Δ mediates the flavor conserving interactions. The absence of muon $(g-2)_\mu$ can be explained by interference effects arising from opposite contributions of Z' and Δ , with similar interference patterns also manifesting in the tau decay process $\tau \rightarrow \mu\nu\bar{\nu}$. These counteracting effects render the model phenomenologically interesting and warrant further investigation. For the mass $m_{Z'}$ in the range of hundreds of GeV, we find that $\mu^+\mu^+$ and μ^+e^- collider at the μ TRISTAN can probe many regions inaccessible to current experiments and offer greater projected sensitivity than opposite-sign muon colliders. This suggests that μ TRISTAN can serve as complementary exploration to the $U(1)_{L_\mu-L_\tau}$ model, providing compelling motivation for the next generation of high-energy lepton colliders.

I. INTRODUCTION

High-energy muon colliders have consistently attracted significant attention over the past decades for studying the Standard Model (SM) and searching for new physics, owing to their high center-of-mass energy and clean lepton collider environment. To date, most muon collider studies have focused on the opposite-sign muon cases [1–24]. The possibility of exploring physics with same-sign muon colliders [25], referred to as μ TRISTAN [26], has recently gained attention. This collider utilizes a low-emittance muon beam originally developed for the muon $g-2$ /EDM experiment at J-PARC [27]. It can accelerate μ^+ and e^- beams up to 1 TeV and 30 GeV, respectively, resulting in the center-of-mass energy of 346 GeV for μ^+e^- and 2 TeV for $\mu^+\mu^+$ collider experiments. The luminosities are estimated to be at the level of 10^{33-34} $\text{cm}^{-2}\text{s}^{-1}$ [26, 28], which makes μ^+e^- collider as an excellent Higgs boson factory and high energy $\mu^+\mu^+$ collider as a promising facility for direct searches of new particles [29–36].

The detection capabilities of opposite-sign and same-sign muon colliders can be compared in a model-independent manner. The effective four-fermion operators are

$$\mathcal{L} = C_{AB}^{ijkl} (\bar{l}_i \gamma^\mu P_A l_j) (\bar{l}_k \gamma^\mu P_B l_l) + h.c. . \quad (1)$$

Here A and B means the chirality projection $P_{L/R} = (1 \mp \gamma_5)/2$, and i, j, k, l are indices of charged lepton flavors e, μ, τ . Take $\mu\mu \rightarrow \tau\tau$ as an example to illustrate, the coefficient should be $C_{AB}^{\tau\mu\tau\mu}$. This leads to the ratio of the cross section at $\mu^+\mu^+$ and $\mu^+\mu^-$ colliders, expressed as [37]

$$\frac{\sigma(\mu^+\mu^+ \rightarrow \tau^+\tau^+)}{\sigma(\mu^+\mu^- \rightarrow \tau^+\tau^-)} = 3 \times \frac{|C_{LL}|^2 + |C_{RR}|^2 + (|C_{LR}|^2 + |C_{RL}|^2)/6}{|C_{LL}|^2 + |C_{RR}|^2 + |C_{LR}|^2 + |C_{RL}|^2} . \quad (2)$$

For simplicity, we omit the superscripts of flavor indices. This clearly indicates that in models where C_{LL} or $C_{RR} \neq 0$, the sensitivity of the $\mu^+\mu^+$ collider could surpass that of the $\mu^+\mu^-$ collider, emphasizing the necessity of analyses involving the $\mu^+\mu^+$ collider.

Recently, FNAL released the latest precise measurements of the muon magnetic moment and combined them with previous results [38, 39] to obtain a new experimental world average, $a_\mu^{exp} = 1165920715(145) \times 10^{-12}$ [40].

* sps_huangf@ujn.edu.cn

† sunjin0810@ibs.re.kr(contact author)

Additionally, the theory community has updated the Standard Model (SM) prediction by considering only lattice-QCD calculations, excluding the data-driven dispersive approach, yielding $a_\mu^{SM} = 116592033(62) \times 10^{-11}$ [41]. The deviation is $a_\mu^{exp} - a_\mu^{SM} = 39(64) \times 10^{-11}$, indicating no significant tension between the SM and experimental results at the current precision level. However, the result requires further analysis due to large uncertainties, and theoretical discrepancies between lattice-QCD calculations and the data-driven dispersive approach. Nevertheless, it also imposes stringent constraints on any new model building. A widely known model, the $L_\mu - L_\tau$ model, is subject to stringent bounds from various experiments in the low-mass region ($m_{Z'} < 70$ GeV), including BaBar for $m_{Z'} \sim (0.2, 10)$ GeV [42, 43], CMS $Z \rightarrow 4\mu$ for $m_{Z'} \sim (5, 70)$ GeV [43–46], BOREXINO for $m_{Z'} \sim (0.01, 1)$ GeV [47, 48], and NA64 μ [49] below 1 GeV. Given the stringent collider bounds in the low-mass region, we focus on the high-mass regime (on the order of hundreds of GeV), where the primary relevant constraints arise from muon neutrino trident (MNT) production [45, 50]. Fortunately, previous studies [51–54] indicate that the MNT bound can be evaded by transforming the original flavor-conserving Z' interaction into a fully off-diagonal form with the assistance of type-II triplets and exchange symmetry. Interestingly, the physical effects of the maximally flavor-violating Z' and the triplet scalars are mutually opposite. For example, the Z' provides a positive contribution to a_μ , whereas the triplet contributes negatively, effectively reinforcing the latest results about the absence. These mutually counteracting effects make the new model mechanism worthy of further study. Previous collider analyses have focused on the opposite-sign muon $\mu^+\mu^-$ collider, including the two-body process $\mu^-\mu^+ \rightarrow \tau^-\tau^+$ and the four-body process $\mu^-\mu^+ \rightarrow \mu^\pm\mu^\pm + \tau^\mp\tau^\mp$ [21]. The new model mechanism can be advantageously explored at the μ TRISTAN collider, as analyzed in Eq. (2).

In this paper, we aim to utilize the $\mu^+\mu^+$ and μ^+e^- colliders to search for a maximally flavor-changing Z' boson within the $L_\mu - L_\tau$ model. The structure of the paper is organized as follows. In section II, we discuss the model construction of the maximal flavor changing $L_\mu - L_\tau$ Z' interactions augmented by triplet scalars. Section III presents the collider signatures, firstly analyzing the two-body case in $\mu^+\mu^+$ collider to fix the triplet effects, followed by an extension to the four-body processes at both the $\mu^+\mu^+$ and μ^+e^- colliders. We provide our conclusions in section IV.

II. THE $U(1)_{L_\mu-L_\tau}$ MODEL FOR MAXIMAL μ - τ COUPLING

In the minimal $U(1)_{L_\mu-L_\tau}$ model, the left-handed $SU(3)_C \times SU(2)_L \times U(1)_Y$ doublets, $L_{L_i} : (1, 2, -1/2)$, and the right-handed singlets, $e_{R_i} : (1, 1, -1)$, transform under the gauged $U(1)_{L_\mu-L_\tau}$ group with charges 0, +1, and -1 for the first, second, and third generations, respectively. The model's Z' gauge boson interacts exclusively with leptons in the weak interaction basis [51, 55]

$$\mathcal{L}_{Z'} = -\tilde{g}(\bar{\mu}\gamma^\mu\mu - \bar{\tau}\gamma^\mu\tau + \bar{\nu}_\mu\gamma^\mu P_L\nu_\mu - \bar{\nu}_\tau\gamma^\mu P_L\nu_\tau)Z'_\mu, \quad (3)$$

where \tilde{g} is the $U(1)_{L_\mu-L_\tau}$ gauge coupling. By introducing a singlet scalar field S with vacuum expectation value (VEV) $v_S/\sqrt{2}$ and a $U(1)_{L_\mu-L_\tau}$ charge +1 to spontaneously break the $U(1)_{L_\mu-L_\tau}$ symmetry, the Z' boson acquires a mass given by $m_{Z'} = \tilde{g}v_S$.

The above interaction is purely flavor-conserving but can be transformed into a fully flavor-changing interaction. We briefly outline the construction of such a model. This requires introducing three Higgs doublets, $H_{1,2,3} : (1, 2, 1/2)$ with vevs $\langle H_i \rangle = v_i/\sqrt{2}$, carrying $U(1)_{L_\mu-L_\tau}$ charges of 0, +2, and -2, respectively. An unbroken exchange symmetry is imposed such that $Z' \rightarrow -Z'$, $H_1 \leftrightarrow H_1$ and $H_2 \leftrightarrow H_3$ with $v_2 = v_3 = v$. Under these conditions, the Z' interactions and Yukawa couplings to leptons are given by

$$\begin{aligned} L_H = & -\tilde{g}(\bar{l}_2\gamma^\mu Ll_2 - \bar{l}_3\gamma^\mu Ll_3 + \bar{e}_2\gamma^\mu Re_2 - \bar{e}_3\gamma^\mu Re_3)Z'_\mu \\ & - [Y_{11}^l \bar{l}_1 Re_1 + Y_{22}^l (\bar{l}_2 Re_2 + \bar{l}_3 Re_3)]H_1 - Y_{23}^l (\bar{l}_2 Re_3 H_2 + \bar{l}_3 Re_2 H_3) + H.C. \end{aligned} \quad (4)$$

After electroweak symmetry breaking, the scalars acquire non-zero VEVs that generate the charged lepton masses

through the Yukawa terms shown in the second line of Eq. (4). However, since the resulting mass matrix is non-diagonal, it must be diagonalized via the following transformation:

$$\begin{pmatrix} \mu \\ \tau \end{pmatrix} = \frac{1}{\sqrt{2}} \begin{pmatrix} 1 & -1 \\ 1 & 1 \end{pmatrix} \begin{pmatrix} e_2 \\ e_3 \end{pmatrix}, \quad (5)$$

After applying the above transformation to the charged lepton mass eigenstate basis, we obtain the desired flavor-changing Z' interactions in the form as

$$\mathcal{L}_{Z'} = -\tilde{g}(\bar{\mu}\gamma^\mu\tau + \bar{\tau}\gamma^\mu\mu + \bar{\nu}_\mu\gamma^\mu L\nu_\tau + \bar{\nu}_\tau\gamma^\mu L\nu_\mu)Z'_\mu. \quad (6)$$

The aforementioned Z' interaction also induces the process $\tau \rightarrow \mu\bar{\nu}_\mu\nu_\tau$, whose effects can be mitigated by introducing three $Y = 1$ scalar triplets, $\Delta_{1,2,3} : (1, 3, 1)$ ($\langle \Delta_i \rangle = v_{\Delta_i}/\sqrt{2}$) with $U(1)_{L_\mu-L_\tau}$ charges $(0, -2, 2)$ [53]. This Δ field is core of the famous type-II seesaw mechanism providing small neutrino masses [56–61] with

$$\Delta = \begin{pmatrix} \Delta^+/\sqrt{2} & \Delta^{++} \\ \Delta^0 & -\Delta^+/\sqrt{2} \end{pmatrix}, \quad \Delta^0 = \frac{v_\Delta + \delta + i\eta}{\sqrt{2}}. \quad (7)$$

Under the above exchange symmetry $\Delta_1 \leftrightarrow \Delta_1$, $\Delta_2 \leftrightarrow \Delta_3$ with $v_{\Delta_2} = v_{\Delta_3}$, we use the transformation in Eq.(5) to obtain the Yukawa terms in terms of the component fields $\Delta^{0,+,++}$ as

$$L_\Delta = -(\bar{\nu}_e^c, \bar{\nu}_\mu^c, \bar{\nu}_\tau^c)M(\Delta^0)L \begin{pmatrix} \nu_e \\ \nu_\mu \\ \nu_\tau \end{pmatrix} + \sqrt{2}(\bar{\nu}_e^c, \bar{\nu}_\mu^c, \bar{\nu}_\tau^c)M(\Delta^+)L \begin{pmatrix} e \\ \mu \\ \tau \end{pmatrix} + (\bar{e}^c, \bar{\mu}^c, \bar{\tau}^c)M(\Delta^{++})L \begin{pmatrix} e \\ \mu \\ \tau \end{pmatrix},$$

with $M(\Delta) = \begin{pmatrix} Y_{11}^\nu\Delta_1 & 0 & 0 \\ 0 & (Y_{22}^\nu(\Delta_2 + \Delta_3) - 2Y_{23}^\nu\Delta_1)/2 & Y_{22}^\nu(\Delta_2 - \Delta_3)/2 \\ 0 & Y_{22}^\nu(\Delta_2 - \Delta_3)/2 & (Y_{22}^\nu(\Delta_2 + \Delta_3) + 2Y_{23}^\nu\Delta_1)/2 \end{pmatrix}.$ (8)

We find that numerous model parameters complicate the analysis. For simplicity, we make the following assumptions:

- $\Delta_2 = \Delta_3$: The degenerate case is enforced by the exchange symmetry, which forbids off-diagonal interactions.
- $Y_{11,23} \ll Y_{22}$: This suppresses the effects of Δ_1 , leaving the triplet contributions dominated by Δ_2 and Δ_3 .
- $m_{\Delta^{+,+,0}} = m_\Delta$: The degeneracy of the triplet components ensures that the triplet scalars have identical masses.

The above assumptions ensure that the triplet effects can be effectively described by the coupling $y = Y_{22}$ and the mass parameter $m_\Delta = m_{\Delta_2} = m_{\Delta_3}$.

III. COLLIDER SIGNATURE ANALYSIS

Note that our models include both the fully flavor-changing Z' interactions and flavor-conserving Δ interactions, characterized by four parameters: \tilde{g} , $m_{Z'}$, y , and m_Δ . However, the combined effects of these four parameters contribute to various physical processes, making it difficult to isolate the individual contributions from Z' or Δ . In this section, we first analyze the decay chains of Δ and Z' to identify their dominant decay channels. Then, we investigate the physical effects of the triplet scalars through the specific process $\mu^+\mu^+ \rightarrow W^+W^+, \mu^+\mu^+$. Finally, we extend the analysis to four-body collider processes involving both Z' and Δ .

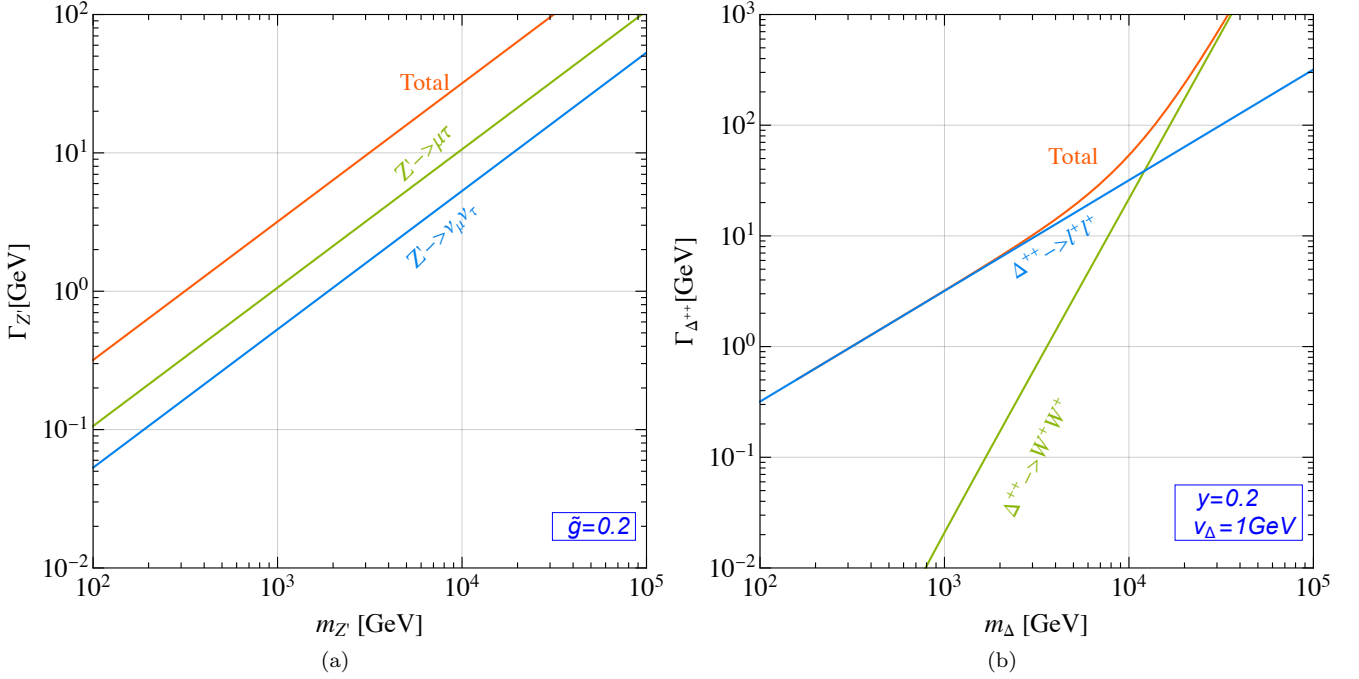


FIG. 1: The decay width as functions of mass in our model. Different decay channels are distinguished by distinct colors. (a) The left panel corresponds to Z' decay width for $\tilde{g} = 0.2$. (b) The right panel means triplet scalar Δ^{++} decay width for $y = 0.2$ and $v_\Delta = 1$ GeV.

A. decay chains of triplet Δ^{++} and Z' bosons

For the Z' gauge boson, it only mediates the flavor changing $\mu - \tau$ interactions, leading to decay chains involving charged leptons and neutrinos. The relevant decay widths are calculated as

$$\begin{aligned} \Gamma_{Z'} &= \Gamma(Z' \rightarrow \mu^+ \tau^-) + \Gamma(Z' \rightarrow \mu^- \tau^+) + \Gamma(Z' \rightarrow \nu_\mu \bar{\nu}_\tau) + \Gamma(Z' \rightarrow \nu_\tau \bar{\nu}_\mu), \\ \Gamma(Z' \rightarrow \mu^\pm \tau^\mp) &= \frac{\tilde{g}^2}{24\pi} \frac{1}{m_{Z'}^5} (m_{Z'}^2 - m_\tau^2)^2 (2m_{Z'}^2 + m_\tau^2), \quad \Gamma(Z' \rightarrow \nu_{\mu(\tau)} \bar{\nu}_{\tau(\mu)}) = \frac{\tilde{g}^2 m_{Z'}}{24\pi}. \end{aligned} \quad (9)$$

Here, we neglect the muon mass. In the limit $m_{Z'} \gg m_\tau$, the decay width into neutrinos is half that of the charged lepton decay, due to the involvement of only left-handed neutrinos. Consequently, the branching ratio satisfies $Br(Z' \rightarrow \text{invisible}) \approx 2/3$, provided the decay channel $Z' \rightarrow \mu\tau$ is kinematically allowed. The corresponding decay widths are presented in Fig. 1(a), with the coupling fixed at $\tilde{g} = 0.2$. For different coupling constants, the decay width can be rescaled as $\Gamma = (\tilde{g}/0.2)^2 \Gamma(\tilde{g} = 0.2)$. This indicates that increasing the coupling \tilde{g} and the mass $m_{Z'}$ both enhance the decay width.

For triplet scalars Δ , the degeneracy of triplet masses forbids decay processes between different triplet components. This implies that the effects can be probed via the decay of the doubly-charged scalar Δ^{++} into SM particles through two distinct decay channels, as follows

$$\begin{aligned} \Gamma_\Delta &= \Gamma(\Delta^{++} \rightarrow W^+ W^+) + \Gamma(\Delta^{++} \rightarrow \ell^+ \ell^+), \\ \Gamma(\Delta^{++} \rightarrow W^+ W^+) &= \frac{G_F^2 v_\Delta^2}{2\pi m_\Delta} [(m_\Delta^2 - 2m_W^2)^2 + 8m_W^4] \sqrt{1 - \frac{4m_W^2}{m_\Delta^2}}, \quad \Gamma(\Delta^{++} \rightarrow \ell^+ \ell^+) = \sum_{\mu, \tau} \frac{y^2 m_\Delta}{8\pi} \sqrt{1 - \frac{4m_\ell^2}{m_\Delta^2}}, \end{aligned} \quad (10)$$

where $G_F = 1.1664 \times 10^{-5} \text{GeV}^{-2}$ is Fermi constant. The decay channel into leptons is proportional to the Yukawa coupling, whereas the decay channel into two W bosons depends on vev. Comparing these two decay modes, we find

that the ratio of their decay widths is given by

$$\frac{\Gamma(\Delta^{++} \rightarrow W^+W^+)}{\Gamma(\Delta^{++} \rightarrow \ell^+\ell^+)} \approx \frac{v_\Delta^2}{v_{SM}^4} \frac{m_\Delta^2}{y^2} \approx 10^{-10} \left(\frac{v_\Delta}{1\text{GeV}}\right)^2 \left(\frac{250\text{GeV}}{v_{SM}}\right)^4 \left(\frac{m_\Delta/\text{GeV}}{y}\right)^2. \quad (11)$$

here we use $G_F = 1/(\sqrt{2}v_{SM}^2)$ with $v_{SM} = 246\text{GeV}$. The corresponding decay widths are presented in Fig. 1(b), where we set $y = 0.2$ and $v_\Delta = 1\text{ GeV}$. For m_Δ below 10 TeV, the dominant decay channel is into charged leptons, $\Delta^{++} \rightarrow \ell^+\ell^+$. Conversely, for $m_\Delta > 10\text{ TeV}$, the dominant decay channel shifts to $\Delta^{++} \rightarrow W^+W^+$. Increasing v_Δ or m_Δ , or decreasing y , enhances the decay into the WW channel. Combining the decay widths of both Z' and Δ^{++} , we find that the widths are generally of order 1 GeV for masses in the hundreds of GeV range. This corresponds to a decay length of approximately 1 fm, indicating that both Z' and Δ^{++} undergo prompt decays.

Before performing a detailed collider analysis, we first examine the corresponding constraints on the model parameters.

- $(g-2)_l$: Exchanging $\Delta^{+,++}$ at one loop level can contribute to electron $(g-2)_l$, while Z' and $\Delta^{+,+}$ provide opposite contributions, expressed as [53, 54]

$$\Delta a_e^\Delta = -\frac{Y_{11}^2}{16\pi^2} \frac{m_e^2}{m_{\Delta_1}^2}, \quad \Delta a_\mu = \Delta a_\mu^{Z'} + \Delta a_\mu^\Delta = \frac{\tilde{g}_{Z'}^2 m_\mu^2}{12\pi^2 m_{Z'}^2} \left(\frac{3m_\tau}{m_\mu} - 2\right) - \frac{m_\mu^2}{16\pi^2} \frac{y_{22}^2}{m_\Delta^2}. \quad (12)$$

Here we adopt the limit $m_{\Delta, Z'} \gg m_{\tau, \mu}$. For $(g-2)_e$, the triplet scalar provides a negative contribution consistent with the measured value $\Delta a_e(C_s) = (-101 + 27) \times 10^{-14}$ [62]. Although our analysis neglects the parameters Y_{11} and Δ_1 for simplicity, viable parameter regions can still accommodate $(g-2)_e$. Furthermore, the opposite contributions from Z' and Δ mutually cancel to comply with the recent muon $(g-2)_\mu$ measurement, $a_\mu = 39(64) \times 10^{-11}$. We apply a 2σ confidence level to impose exclusion limits on the model parameters in the $\epsilon - m_{Z'}$ plane, shown in the upper left corner of Fig. 4.

- $\tau \rightarrow \mu\nu\bar{\nu}$: The decay processes are mediated by Z' and Δ^+ effects in terms of the ratios as [53, 54]

$$R^\tau \equiv \frac{\Gamma(\tau^- \rightarrow \mu^- \bar{\nu}_\mu \nu_\tau)}{\Gamma(\tau^- \rightarrow \mu^- \bar{\nu}_\mu \nu_\tau)_{SM}} = \left(1 - \frac{4m_W^2}{g^2} \frac{y_{22}^2}{4m_{\Delta^+}^2}\right)^2 + \frac{4m_W^2}{g^2} \frac{\tilde{g}^2}{m_{Z'}^2} \left(1 - \frac{4m_W^2}{g^2} \frac{y_{22}^2}{4m_{\Delta^+}^2}\right) + \frac{\tilde{g}^4}{g^4} \frac{4m_W^4}{m_{Z'}^4}. \quad (13)$$

Combining the SM predictions $R_{SM}^\tau = 0.972564 \pm 0.00001$ [63] and average experimental values $R_{aver}^\tau = 0.972968 \pm 0.002233$ from HFLAV collaboration [64] and Belle-II [65], the ratio can be obtained as $R^\tau = 1.00042 \pm 0.00230$, which imposes the stringent bounds as shown in the Fig. 4.

- **collider bounds:** Current constraints on the degenerate triplet scalar set a lower mass limit of $m_\Delta > 420\text{ GeV}$ for $\Delta m = 0$ and $v_\Delta \sim \mathcal{O}(\text{GeV})$ [66].
- **Neutrino trident processes:** The process $\nu_\mu + N \rightarrow \nu_{\mu, \tau} + N + \mu^+ \mu^-$ can be induced by Δ^+ at tree-level as [53, 54]

$$\frac{\sigma_{\Delta^+}}{\sigma_{SM}}|_{trident} = \frac{\left(1 + 4s_W^2 - \frac{m_W^2}{g^2} \frac{2y_{22}^2}{m_\Delta^2}\right)^2 + \left(1 - \frac{m_W^2}{g^2} \frac{2y_{22}^2}{m_\Delta^2}\right)^2}{[(1 + 4s_W^2)^2 + 1]}, \quad (14)$$

Combining the current bounds from CHARM, CCFR and NuTeV [67–69], the averaged value is 0.95 ± 0.25 , which can place an upper bound $y^2/m_\Delta^2 < 2 \times 10^{-5}\text{ GeV}^{-2}$.

B. two-body final states

Given the interplay between the two new particles (Z' and Δ), we aim to disentangle their overlapping effects by analyzing distinct scattering processes. In certain processes, only the triplet scalar Δ contributes, while Z' does not, such as $\mu^+\mu^+ \rightarrow W^+W^+$ and $\mu^+\mu^+ \rightarrow \mu^+\mu^+$. Therefore, these two processes provide an ideal platform to constrain the viable parameter space of the triplet Δ .

1. Identify the triplet effects

In order to isolate the effects of the triplet scalar, we focus on processes solely mediated by it, specifically $\mu^+\mu^+ \rightarrow W^+W^+$ and $\mu^+\mu^+ \rightarrow \mu^+\mu^+$.

In the $\mu^+\mu^+ \rightarrow W^+W^+$ process, the mediation occurs exclusively via the s -channel exchange of the doubly-charged scalar Δ^{++} . The corresponding cross section is computed as follows [37]

$$\sigma(\mu^+\mu^+ \rightarrow W^+W^+) = \frac{G_F^2 y^2 v_\Delta^2}{2\pi} \frac{(s - 2m_W^2)^2 + 8m_W^4}{(s - m_\Delta^2)^2 + m_\Delta^2 \Gamma_\Delta^2} \sqrt{1 - \frac{4m_W^2}{s}}, \quad (15)$$

Here, s denotes the center-of-mass (COM) energy. The cross section is found to depend on the v_Δ , the mass m_Δ , and the coupling constant y . Assuming an integrated luminosity of $\mathcal{L} = 12fb^{-1}$ [26] [26], we derive constraints by requiring the number of signal events to satisfy $N_{sig} = \mathcal{L} \times \sigma \geq 3$. The corresponding bounds are illustrated in Fig.2. The green regions represent phenomenological constraints on the model parameters [53, 54], including those from $(g-2)_\mu$, MNT production, and $\tau \rightarrow \mu\nu\nu$ decay. The gray regions indicate limits arising from the degenerate triplet scalar mass bound $m_\Delta > 420$ GeV [66] and perturbativity constraint $y \leq \sqrt{4\pi}$. We analyze three distinct scenarios corresponding to triplet VEV values of $v_\Delta = 0.03, 0.5, \text{ and } 3.5$ GeV, marked by the red regions. Our results show that, to observe a viable signal, the triplet VEV should lie within the range $(0.03 - 3.5)$ GeV. The upper limit of 3.5 GeV is set by the electroweak ρ parameter at the 3σ confidence level [70]. For $v_\Delta = 0.03$ GeV, the allowed triplet scalar mass peaks near $m_\Delta \sim \sqrt{s} = 2$ TeV. To streamline subsequent analyses of various collider processes, we select benchmark parameters indicated by a yellow star: $y = 0.25, m_\Delta = 500$ GeV, and $v_\Delta = 1$ GeV.

The process $\mu^+\mu^+ \rightarrow \mu^+\mu^+$ conserves charged lepton flavor, implying the presence of SM background contributions. The total amplitude consists of three components: the SM contribution (mediated by $h, Z,$ and γ in the t - and u -channels), the new physics (NP) contribution (via s -channel exchange of Δ^{++}), and the interference between them. Consequently, the total cross section comprises the pure SM, pure NP, and interference terms. A direct calculation of the cross section reveals that $\sigma(t)$ exhibits an infrared divergence, particularly in the limit where the Mandelstam variable $t \rightarrow 0$ or $t \rightarrow -s$. This is due to the fact that the interference term includes one term proportional to $\ln(t/(t+s))$. In order to obtain the finite results, we can impose the cuts by considering the bounds on rapidity $|\eta| < 2.5$, which is commonly used in the detector-level simulations. The rapidity has the relation with variable t as

$$t = -\frac{s}{1 + e^{-2\eta}} \rightarrow t \in \left[-\frac{s}{1 + e^{-2\eta_{\max}}}, -\frac{s}{1 + e^{2\eta_{\max}}} \right] \quad (16)$$

Here we neglect the muon mass in this analysis. By setting the rapidity cut to $\eta_{\max} = 2.5$, we compute the cross section for the benchmark values $y = 0.25$ and $m_\Delta = 500$ GeV, as shown in Fig. 3(a). The individual contributions are represented by different colors: the total cross section σ_{total} (orange), the pure triplet contribution σ_Δ (green), the SM contribution σ_{SM} (blue), and the SM-triplet interference term $\sigma_{\text{SM}-\Delta}$ (red). We find that the SM contribution dominates across the full range of \sqrt{s} , except near the resonance at $\sqrt{s} \sim m_\Delta$, where the enhancement is due to the s -channel mediation of Δ^{++} resonance. The interference term is positive when $\sqrt{s} < m_\Delta$, and becomes negative for $\sqrt{s} > m_\Delta$. In particular, at $\sqrt{s} = 2$ TeV, the SM contribution significantly dominates, exceeding the sub-dominant interference term by approximately two orders of magnitude.

In order to extract signatures in cases involving the SM background, we need to adopt the following criteria as

$$CL = \frac{S}{\sqrt{S+B}} = \frac{\mathcal{L}|\sigma_S|}{\sqrt{\mathcal{L}(\sigma_S + \sigma_B)}} = \sqrt{\mathcal{L}} \frac{|\sigma_S|}{\sqrt{(\sigma_S + \sigma_B)}} \geq 3. \quad (17)$$

The relevant bounds are shown in blue in Fig. 2. We find that there exist some parameter regions for Δ that simultaneously satisfy both phenomenological constraints and collider sensitivity, such as the benchmark point $y = 0.25, m_\Delta = 500$ GeV, and $v_\Delta = 1$ GeV.

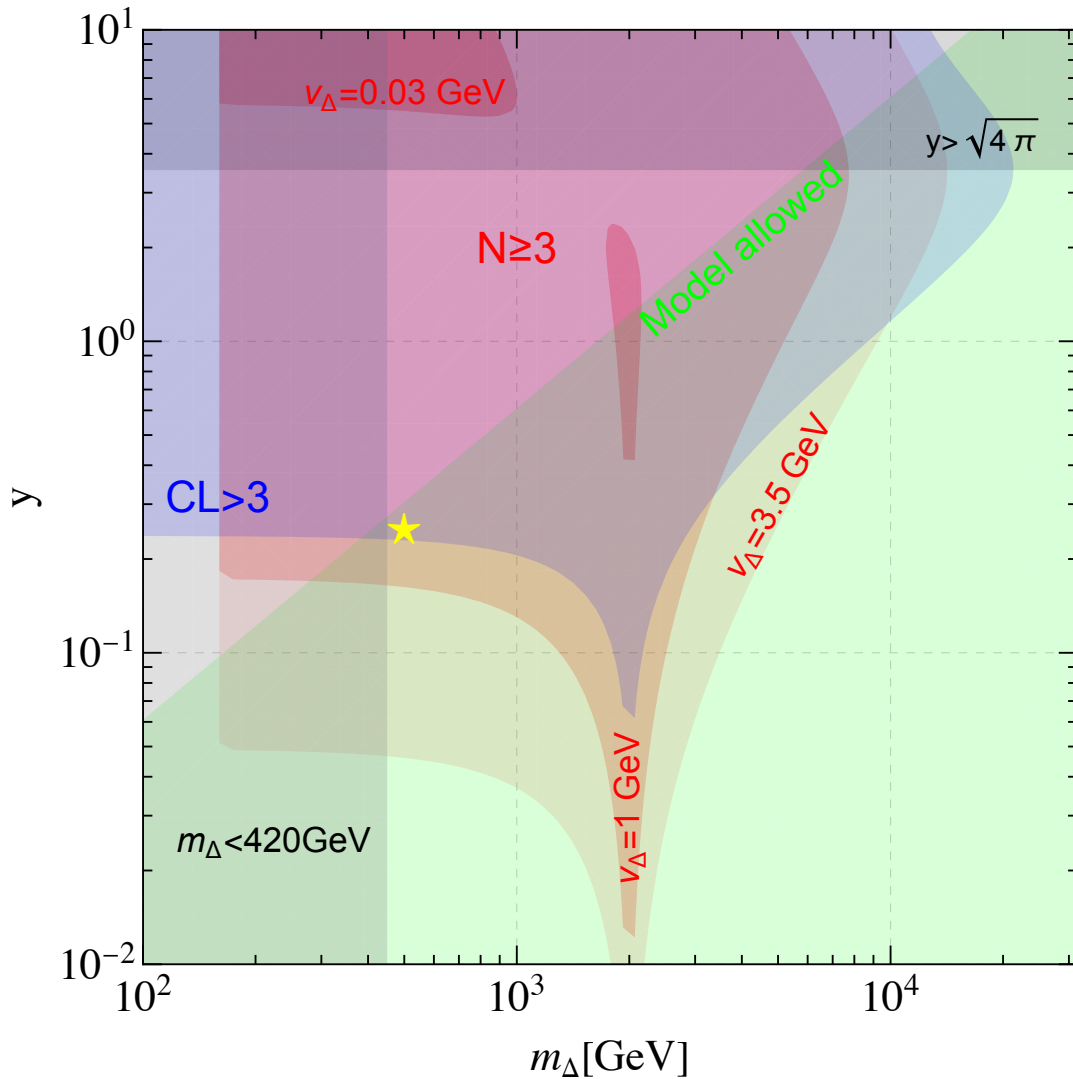


FIG. 2: The allowed parameter space for the triplet scalars in the m_Δ - y plane. Different constraints are indicated using distinct colors: green for phenomenological limits (from $(g-2)_\mu$, MNT production, and $\tau \rightarrow \mu\nu\bar{\nu}$) [54]; red for regions satisfying $N(\mu^+\mu^+ \rightarrow W^+W^+) \geq 3$ under three representative values of $v_\Delta = (0.03, 1, 3.5)$ GeV; blue for $CL(\mu^+\mu^+ \rightarrow \mu^+\mu^+) \geq 3$ as defined in Eq.(17); and gray for excluded regions due to the perturbativity condition $y \leq \sqrt{4\pi}$ and the lower bound on the degenerate triplet scalar mass $m_\Delta > 420$ GeV[66]. The yellow star denotes the chosen benchmark point: $y = 0.25$, $m_\Delta = 500$ GeV, and $v_\Delta = 1$ GeV.

2. $\mu^+\mu^+ \rightarrow \tau^+\tau^+$

For $\mu^+\mu^+ \rightarrow \tau^+\tau^+$, it involves simultaneous charged lepton flavor violation and lepton number violation. This feature implies the absence of SM background contributions, rendering it a promising collider signature at the two-body level within our model. The flavor-changing Z' model incorporating a triplet scalar can contribute to this process via two distinct mechanisms: Δ^{++} mediated s -channel and Z' mediated t - and u -channels. The corresponding

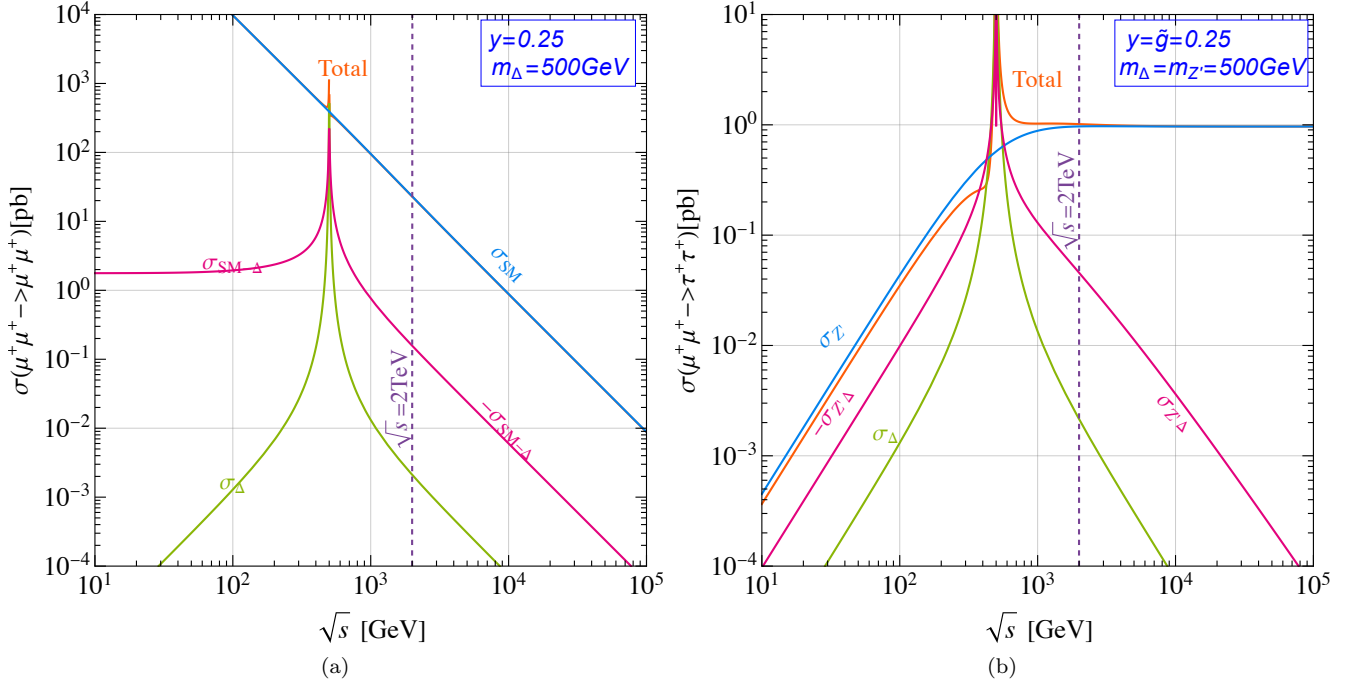


FIG. 3: The cross section of $\mu^+\mu^+ \rightarrow \ell^+\ell^+$ with \sqrt{s} . The contributions from individual components are shown in different colors. The center-of-mass energy of μ TRISTAN, $\sqrt{s} = 2$ TeV, is indicated by the dashed line. (a) The left panel corresponds to the case of $\mu^+\mu^+ \rightarrow \mu^+\mu^+$ with $y = 0.25$ and $m_\Delta = 500$ GeV. (b) The right panel means the case of $\mu^+\mu^+ \rightarrow \tau^+\tau^+$ with $y = \tilde{g} = 0.25$, $m_\Delta = m_{Z'} = 500$ GeV.

scattering amplitudes are

$$\begin{aligned}
 M_s &= \frac{1}{2} \frac{y^2}{s - m_\Delta^2 + im_\Delta \Gamma_\Delta} \bar{\mu}(p_1) \gamma^\mu P_L \tau(p_4) \bar{\mu}(p_2) \gamma_\mu P_L \tau(p_3), \\
 M_t &= -\frac{\tilde{g}^2}{t - m_{Z'}^2 + im_{Z'} \Gamma_{Z'}} \bar{\mu}(p_1) \gamma^\mu \tau(p_3) \bar{\mu}(p_2) \gamma_\mu \tau(p_4), \\
 M_u &= \frac{\tilde{g}^2}{u - m_{Z'}^2 + im_{Z'} \Gamma_{Z'}} \bar{\mu}(p_1) \gamma^\mu \tau(p_4) \bar{\mu}(p_2) \gamma_\mu \tau(p_3).
 \end{aligned} \tag{18}$$

here the momenta of initial state μ^+ and final state τ^+ are denoted as $p_{1,2}$ and $p_{3,4}$. The Mandelstam variables are denoted by s , t , and u and Fierz transformations are applied. Using FeynCalc [71], we calculate the cross section as the sum of the following three terms

$$\begin{aligned}
 \sigma(\mu^+\mu^+ \rightarrow \tau^+\tau^+) &= \sigma_\Delta + \sigma_{Z'} + \sigma_{Z'\Delta}, \\
 \sigma_\Delta &= \frac{y^4}{64\pi} \frac{s}{(s - m_\Delta^2)^2 + \Gamma_\Delta^2 m_\Delta^2}, \\
 \sigma_{Z'} &= \frac{\tilde{g}^4}{4\pi s} \left[1 + \frac{m_{Z'}^2 (2m_{Z'}^2 + 3s)}{s(2m_{Z'}^2 + s)} \log \frac{m_{Z'}^2 (\Gamma_{Z'}^2 + m_{Z'}^2)}{\Gamma_{Z'}^2 m_{Z'}^2 + (m_{Z'}^2 + s)^2} + \frac{(m_{Z'}^4 + m_{Z'}^2 (2s - \Gamma_{Z'}^2) + 2s^2)}{s\Gamma_{Z'} m_{Z'}} \tan^{-1} \left(\frac{s\Gamma_{Z'}/m_{Z'}}{(s + m_{Z'}^2 + \Gamma_{Z'}^2)} \right) \right], \\
 \sigma_{Z'\Delta} &= \frac{y^2 \tilde{g}^2}{16\pi (s - m_\Delta^2)^2 + \Gamma_\Delta^2 m_\Delta^2} \left[2\Gamma_\Delta m_\Delta \tan^{-1} \left(\frac{s\Gamma_{Z'}/m_{Z'}}{(s + m_{Z'}^2 + \Gamma_{Z'}^2)} \right) - (s - m_\Delta^2) \log \frac{m_{Z'}^2 (\Gamma_{Z'}^2 + m_{Z'}^2)}{\Gamma_{Z'}^2 m_{Z'}^2 + (m_{Z'}^2 + s)^2} \right].
 \end{aligned} \tag{19}$$

Here we ignore the charged lepton masses of both the initial and final states. The symbols σ_Δ and $\sigma_{Z'}$ denote the s -channel Δ and the t - and u -channel Z' contributions, respectively, while $\sigma_{Z'\Delta}$ represents the interference term between Δ and Z' . Additionally, in certain scenarios, the interference term can be negative, particularly when $\sqrt{s} < m_\Delta$.

Analyzing the structure of the cross section, we find that in certain limits it approximates to

$$\sigma(\mu^+\mu^+ \rightarrow \tau^+\tau^+) \propto \begin{cases} \frac{y^4}{\Gamma_\Delta^2}, & \text{for } \sqrt{s} \simeq m_\Delta, \\ \frac{\tilde{g}^4}{m_{Z'}^2}, & \text{for } \sqrt{s} \gg m_{Z'}, \\ \tilde{g}^4 \frac{s}{m_{Z'}^2}, & \text{for } \sqrt{s} \ll m_{Z'}, \end{cases} \quad (20)$$

The analytic expressions of the cross section given in Eq.(19) as a function of \sqrt{s} , including its different components, are illustrated in Fig.3(b). Here, we set $y = \tilde{g} = 0.25$ and $m_\Delta = m_{Z'} = 500$ GeV. We find that at large \sqrt{s} , the dominant contribution arises from Z' , which exceeds the Δ contribution by approximately two orders of magnitude and the interference terms by about three orders of magnitude. The Δ contribution dominates only when $\sqrt{s} \sim m_\Delta$, as indicated in Eq. (20). Additionally, for $\sqrt{s} < m_\Delta$, negative interference terms arise, partially canceling contributions from the pure Z' and Δ channels. Fortunately, for the chosen benchmark points and at $\sqrt{s} = 2$ TeV, the negative interference scenario does not occur. Requiring the event numbers $N = \sigma \cdot \mathcal{L} \geq 3$, we can obtain the corresponding sensitivity indicated by the red regions in Fig. 4.

C. Four-body final states

Considering the prompt decays of Z' and Δ^{++} , the produced Z' and Δ^{++} will undergo subsequent decays rapidly. Pair production occurs only at opposite-sign muon colliders $\mu^+\mu^-$, which has been studied in Ref. [21]. Therefore, we primarily focus on single production at μ TRISTAN followed by subsequent prompt decays, particularly targeting four visible charged-lepton final states exhibiting clear lepton flavor and generation number violation. These processes four-body final states include $\mu^+\mu^+ \rightarrow \mu^+\tau^+Z'(\rightarrow \tau^+\mu^-)$, $\mu^+\mu^+ \rightarrow \mu^+\mu^-\Delta^{++}(\rightarrow \tau^+\tau^+)$, $\mu^+\mu^+ \rightarrow \mu^+\mu^-\tau^+\tau^+$, $e^-\mu^+ \rightarrow e^-\tau^+Z'(\rightarrow \tau^+\mu^-)$, $e^-\mu^+ \rightarrow e^-\mu^-\Delta^{++}(\rightarrow \tau^+\tau^+)$ and $e^-\mu^+ \rightarrow e^-\mu^-\tau^+\tau^+$.

TABLE I: The signal event numbers for different collider processes. Here we choose $y = 0.25$ and $m_\Delta = 500$ GeV. The symbol with “-” denotes kinematically forbidden processes.

Facility	\sqrt{s} (GeV)	\mathcal{L}_{lum} (ab ⁻¹)	Process	Event numbers			
				$\tilde{g} = 0.05$		$\tilde{g} = 0.3$	
				$m_{Z'} = 200$ GeV	$m_{Z'} = 500$ GeV	$m_{Z'} = 200$ GeV	$m_{Z'} = 500$ GeV
$\mu^+\mu^+$	2000	0.012	$\tau^+\tau^+$	3.70	2.18	8163.75	191.93
			$\mu^+\tau^+Z'(\rightarrow \tau^+\mu^-)$	22.13	8.82	12420.8	3007.33
			$\mu^+\mu^-\Delta^{++}(\rightarrow \tau^+\tau^+)$	111.58	112.22	111.88	112.03
			$\mu^+\mu^-\tau^+\tau^+$	0.15	0.12	270.72	156.45
μ^+e^-	346	1	$e^-\tau^+Z'(\rightarrow \tau^+\mu^-)$	5.99	-	7791.54	-
			$e^-\mu^-\Delta^{++}(\rightarrow \tau^+\tau^+)$	-	-	-	-
			$e^-\mu^-\tau^+\tau^+$	1.68	0	5689.69	2.08

Given the complexity of the four-body final state, we utilize MadGraph to perform a detailed collider analysis. First, we implement the model interactions using FeynRules [72] to generate a Universal FeynRules Output (UFO) model [73] based on the model Lagrangian. Then, we feed the model into MadGraph5-aMC@NLO [74] for all simulations, using PYTHIA 8 [75] for parton showering and hadronization, and DELPHES [76] for fast detector simulation. The following basic cuts are also imposed: (i) transverse momentum $p_T > 10$ GeV, (ii) absolute pseudo-rapidity $|\eta| < 2.5$, (iii) the separation of the two leptons $\Delta R = \sqrt{(\Delta\eta)^2 + (\Delta\phi)^2} > 0.4$. The relevant signal event numbers for various collider processes are presented in Table I.

The collider analysis for four-body final states is organized as follows:

- $\mu^+\mu^+ \rightarrow \mu^+\tau^+Z'(\rightarrow \tau^+\mu^-)$: It involves the on-shell single emission of a Z' boson from one of the initial-state μ^+ , followed by its subsequent decay. The decays into $\mu^+\tau^-$ and $\mu^-\tau^+$ have equal branching ratios. For

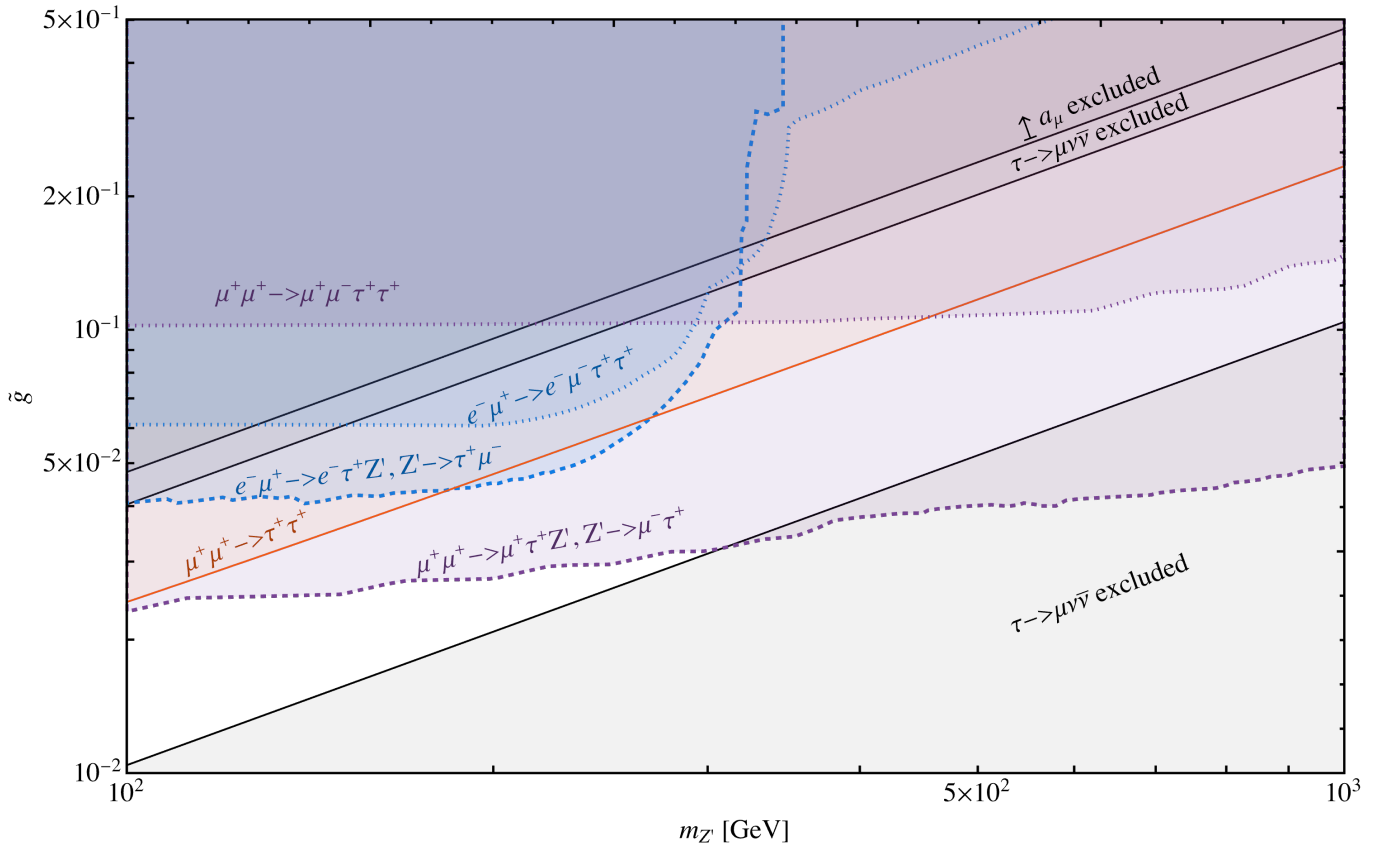


FIG. 4: Current experimental bounds and future μ TRISTAN sensitivities in the $m_{Z'}-\tilde{g}$ plane. The benchmark values are fixed at $y = 0.25$ and $m_\Delta = 500$ GeV. The gray areas indicate exclusion limits derived from $(g-2)_\mu$ [40, 41] and $\tau \rightarrow \mu\nu\bar{\nu}$ [53, 54]. Different collider processes are depicted in distinct colors, with on-shell contributions (dashed) and processes without intermediate states (dotted).

simplicity, we focus primarily on the decay channel $Z' \rightarrow \tau^+\mu^-$, due to its charged lepton flavor violation signature.

- $\mu^+\mu^+ \rightarrow \mu^+\mu^-\Delta^{++}(\rightarrow \tau^+\tau^+)$: One of the initial-state μ^+ emits an on-shell Δ^{++} , which decays promptly. Similarly, the decays into muon and tau flavors share identical branching ratios. However, only the decays into tau flavors violate charged lepton flavor conservation.
- $\mu^+\mu^+ \rightarrow \mu^+\mu^-\tau^+\tau^+$: This process clearly violates charged lepton flavor conservation. Since there are no intermediate on-shell states, the process receives contributions from both Δ and Z' , whether on-shell or off-shell.
- $e^-\mu^+ \rightarrow e^-\tau^+Z'(\rightarrow \tau^+\mu^-)$: It involves the on-shell single emission of a Z' boson from μ^+ , followed by its decay into $\mu^-\tau^+$, exhibiting charged lepton flavor violation. Note that on-shell production requires $m_{Z'} < \sqrt{s}$, meaning the process only probes mass regions below the COM \sqrt{s} .
- $e^-\mu^+ \rightarrow e^-\mu^-\Delta^{++}(\rightarrow \tau^+\tau^+)$: On-shell production of Δ is forbidden since its lower mass bound, $m_\Delta > 420$ GeV, exceeds the center-of-mass energy $\sqrt{s} = 346$ GeV.
- $e^-\mu^+ \rightarrow e^-\mu^-\tau^+\tau^+$: This process does not involve any on-shell intermediate states, meaning it is influenced by off-shell Δ^{++} and either on-shell or off-shell Z' . The combined effects of both contribute jointly to the process.

The relevant findings are illustrated in Fig. 4, showing both current bounds (light gray regions) and projected sensitivities of μ TRISTAN colliders (colored regions). The gray regions summarize current experimental constraints, as mentioned earlier, including muon $(g-2)_\mu$ and $\tau \rightarrow \mu\nu\bar{\nu}$. We find that the decay $\tau \rightarrow \mu\nu\bar{\nu}$ provides significantly more stringent bounds than the muon $(g-2)_\mu$. Although a large portion of the parameter space has already been excluded, some viable regions remain to be explored at colliders.

The colored regions represent the projected sensitivities from various collider processes at μ TRISTAN. These are derived by requiring the number of events $N = \sigma \cdot \mathcal{L} > 3$. Our analysis demonstrates that these processes can probe new parameter regions that remain unconstrained by current experimental bounds. For the two-body process $\mu^+\mu^+ \rightarrow \tau^+\tau^+$, the coupling $\tilde{g} \sim 0.025$ can be probed, which improves sensitivity by approximately a factor of two compared to the bounds from $\tau \rightarrow \mu\nu\bar{\nu}$. For on-shell Z' production, indicated by the dashed line, the process $e^-\mu^+ \rightarrow e^-\tau^+Z'(\rightarrow \tau^+\mu^-)$ can achieve sensitivity around $\tilde{g} \sim 0.04$ for $m_{Z'} < 346$ GeV, while $\mu^+\mu^+ \rightarrow \mu^+\tau^+Z'(\rightarrow \tau^+\mu^-)$ can reach down to $\tilde{g} \sim 0.024$. Moreover, $\mu^+\mu^+ \rightarrow \mu^+\tau^+Z'(\rightarrow \tau^+\mu^-)$ provides significantly better sensitivity across the entire mass range, fully covering the regions probed by both $e^-\mu^+ \rightarrow e^-\tau^+Z'(\rightarrow \tau^+\mu^-)$ and $\mu^+\mu^+ \rightarrow \tau^+\tau^+$. In scenarios without intermediate states, $\mu^+\mu^+ \rightarrow \mu^+\mu^-\tau^+\tau^+$, the coupling can reach $\tilde{g} \sim 0.1$ across the entire mass region, which is fully covered by the previous scenario involving an on-shell Z' . This suggests the presence of negative interference between the Z' and Δ contributions, which significantly reduces the cross section.

IV. CONCLUSION

In this work, we investigate the detection prospects of the $U(1)_{L_\mu-L_\tau}$ model with triplet scalars Δ at the μ TRISTAN collider. The model framework features maximal flavor-changing $U(1)_{L_\mu-L_\tau}$ Z' interactions alongside flavor-conserving Δ interactions. Both contribute to the muon $(g-2)_\mu$ and the decay $\tau \rightarrow \mu\nu\bar{\nu}$ with opposite effects, which can explain the recent absence of $(g-2)_\mu$ anomaly while satisfying the stringent constraints from tau decay. These counteracting effects render the model phenomenologically interesting and warrant further collider search analyses. Given that the same-sign muon collider offers advantages over the opposite-sign muon collider, we focus on the sensitivity of μ TRISTAN through various charged lepton flavor violation processes. We find that for $m_{Z'}$ in the hundreds of GeV range, the $\mu^+\mu^+$ and μ^+e^- collider modes at μ TRISTAN can probe parameter regions inaccessible to current experiments and offer greater projected sensitivity than opposite-sign muon colliders, especially for processes like $\mu^+\mu^+ \rightarrow \mu^+\tau^+Z'(\rightarrow \tau^+\mu^-)$. This suggests that μ TRISTAN can serve as a complementary probe of the $U(1)_{L_\mu-L_\tau}$ model, providing strong motivation for the next generation of high-energy lepton colliders.

Acknowledgments

The work of Fei Huang is supported by Natural Science Foundation of Shandong Province under Grant No.ZR2024QA138, and Jin Sun is supported by IBS under the project code, IBS-R018-D1..

-
- [1] T. Han, S. Li, S. Su, W. Su, and Y. Wu, *BSM Higgs Production at a Muon Collider*, in *Snowmass 2021*, 5, 2022. [arXiv:2205.11730](#).
 - [2] A. Azatov, F. Garosi, A. Greljo, D. Marzocca, J. Salko, and S. Trifinopoulos, *New physics in $b \rightarrow s\mu\mu$: FCC-hh or a muon collider?*, *JHEP* **10** (2022) 149, [[arXiv:2205.13552](#)].
 - [3] P. M. Brecht, W. Kilian, J. Reuter, and P. Stenemeier, *NLO electroweak corrections to multi-boson processes at a muon collider*, *JHEP* **12** (2022) 138, [[arXiv:2208.09438](#)].
 - [4] J. Arakawa, A. Rajaraman, T. Sui, and T. M. P. Tait, *Probing Muon $g-2$ at a Future Muon Collider*, *SciPost Phys.* **16** (2024), no. 3 072, [[arXiv:2208.14464](#)].

- [5] G.-S. Lv, X.-M. Cui, Y.-Q. Li, and Y.-B. Liu, *Pair production of the vectorlike top partner at future muon collider*, Nucl. Phys. B **985** (2022) 116016.
- [6] J. Reuter, T. Han, W. Kilian, N. Kreher, Y. Ma, T. Striegl, and K. Xie, *Precision test of the muon-Higgs coupling at a high-energy muon collider*, PoS ICHEP2022 (2022) 1239, [[arXiv:2212.01323](#)].
- [7] T. H. Kwok, L. Li, T. Liu, and A. Rock, *Searching for heavy neutral leptons at a future muon collider*, Phys. Rev. D **110** (2024), no. 7 075009, [[arXiv:2301.05177](#)].
- [8] P. Li, Z. Liu, and K.-F. Lyu, *Heavy neutral leptons at muon colliders*, JHEP **03** (2023) 231, [[arXiv:2301.07117](#)].
- [9] T. Li, C.-Y. Yao, and M. Yuan, *Revealing the origin of neutrino masses through the Type II Seesaw mechanism at high-energy muon colliders*, JHEP **03** (2023) 137, [[arXiv:2301.07274](#)].
- [10] S. C. Inan and A. V. Kisselev, *Probe of a Randall–Sundrum-like model from muon pair production at a high-energy muon collider*, J. Phys. G **52** (2025), no. 2 025004, [[arXiv:2301.08585](#)].
- [11] C.-T. Lu, X. Luo, and X. Wei, *Exploring muonphilic ALPs at muon colliders*, Chin. Phys. C **47** (2023), no. 10 103102, [[arXiv:2303.03110](#)].
- [12] S. P. Maharathy and M. Mitra, *Type-II see-saw at $\mu+\mu-$ collider*, Phys. Lett. B **844** (2023) 138105, [[arXiv:2304.08732](#)].
- [13] J. Reuter, *Precision test of the muon-Higgs coupling at a high-energy muon collider*, PoS CORFU2022 (2023) 107, [[arXiv:2305.12814](#)].
- [14] H. Amarkhail, S. C. Inan, and A. V. Kisselev, *Probing anomalous $\gamma\gamma\gamma\gamma$ couplings at a future muon collider*, Nucl. Phys. B **1005** (2024) 116592, [[arXiv:2306.03653](#)].
- [15] A. Belyaev, R. S. Chivukula, B. Fuks, E. H. Simmons, and X. Wang, *Vectorlike top quark production via an electroweak dipole moment at a muon collider*, Phys. Rev. D **108** (2023), no. 3 035016, [[arXiv:2306.11097](#)].
- [16] J.-C. Yang, Y.-C. Guo, and Y.-F. Dong, *Study of the gluonic quartic gauge couplings at muon colliders*, Commun. Theor. Phys. **75** (2023), no. 11 115201, [[arXiv:2307.04207](#)].
- [17] M. Belfkir, T. A. Chowdhury, and S. Nasri, *Doubly-charged scalars of the minimal left-right symmetric model at muon colliders*, Phys. Lett. B **852** (2024) 138605, [[arXiv:2307.16111](#)].
- [18] M. Forsslund and P. Meade, *Precision Higgs width and couplings with a high energy muon collider*, JHEP **01** (2024) 182, [[arXiv:2308.02633](#)].
- [19] E. Loisa, *Searching for the flavon at current and future colliders*, PoS FPCP2023 (8, 2023) 066, [[arXiv:2308.05578](#)].
- [20] Z. Liu, K.-F. Lyu, I. Mahbub, and L.-T. Wang, *Top Yukawa coupling determination at high energy muon collider*, Phys. Rev. D **109** (2024), no. 3 035021, [[arXiv:2308.06323](#)].
- [21] J. Sun, F. Huang, and X.-G. He, *Muon collider signatures for a Z' with a maximal $\mu-\tau$ coupling in $U(1)L\mu-L\tau$* , Phys. Lett. B **845** (2023) 138121.
- [22] B. A. Ouazghour, A. Arhrib, K. Cheung, E.-s. Ghourmin, and L. Rahili, *Comparison between $\mu-\mu+$ and $e-e+$ colliders for charged Higgs production in the 2HDM*, Phys. Rev. D **109** (2024), no. 11 115009, [[arXiv:2308.15664](#)].
- [23] N. Ghosh, S. K. Rai, and T. Samui, *Search for a leptoquark and vector-like lepton in a muon collider*, Nucl. Phys. B **1004** (2024) 116564, [[arXiv:2309.07583](#)].
- [24] O. Mikulenko and M. Marinichenko, *Measuring lepton number violation in heavy neutral lepton decays at the future muon collider*, JHEP **01** (2024) 032, [[arXiv:2309.16837](#)].
- [25] C. A. Heusch and F. Cuyper, *Physics with like-sign muon beams in a TeV muon collider*, AIP Conf. Proc. **352** (1996) 219–231, [[hep-ph/9508230](#)].
- [26] Y. Hamada, R. Kitano, R. Matsudo, H. Takaura, and M. Yoshida, *μ TRISTAN*, PTEP **2022** (2022), no. 5 053B02, [[arXiv:2201.06664](#)].
- [27] M. Abe et al., *A New Approach for Measuring the Muon Anomalous Magnetic Moment and Electric Dipole Moment*, PTEP **2019** (2019), no. 5 053C02, [[arXiv:1901.03047](#)].
- [28] Y. Hamada, R. Kitano, R. Matsudo, and H. Takaura, *Precision $\mu+\mu+$ and $\mu+e-$ elastic scatterings*, PTEP **2023** (2023), no. 1 013B07, [[arXiv:2210.11083](#)].
- [29] R. Jiang, T. Yang, S. Qian, Y. Ban, J. Li, Z. You, and Q. Li, *Searching for Majorana neutrinos at a same-sign muon collider*, Phys. Rev. D **109** (2024), no. 3 035020, [[arXiv:2304.04483](#)].
- [30] T. Li, C.-Y. Yao, and M. Yuan, *Searching for heavy neutral lepton and lepton number violation through VBS at high-energy muon colliders*, JHEP **09** (2023) 131, [[arXiv:2306.17368](#)].
- [31] J.-L. Yang, C.-H. Chang, and T.-F. Feng, *Leptonic di-flavor and di-number violation processes at high energy colliders**, Chin. Phys. C **48** (2024), no. 4 043101, [[arXiv:2302.13247](#)].
- [32] H. Fukuda, T. Moroi, A. Niki, and S.-F. Wei, *Search for WIMPs at future $\mu^+\mu^+$ colliders*, JHEP **02** (2024) 214, [[arXiv:2310.07162](#)].
- [33] P. S. B. Dev, J. Heeck, and A. Thapa, *Neutrino mass models at μ TRISTAN*, Eur. Phys. J. C **84** (2024), no. 2 148, [[arXiv:2309.06463](#)].
- [34] A. Goudelis, J. Kriewald, E. Pinsard, and A. M. Teixeira, *$cLFV$ leptophilic Z' as a dark matter portal: prospects for colliders*, Eur. Phys. J. C **84** (2024), no. 8 804, [[arXiv:2312.14103](#)].
- [35] A. Das and Y. Orikasa, *Z' induced forward dominant processes in μ TRISTAN experiment*, Phys. Lett. B **851** (2024) 138577, [[arXiv:2401.00696](#)].
- [36] G. Lichtenstein, M. A. Schmidt, G. Valencia, and R. R. Volkas, *Complementarity of μ TRISTAN and Belle II in searches for charged-lepton flavour violation*, Phys. Lett. B **845** (2023) 138144, [[arXiv:2307.11369](#)].
- [37] K. Fridell, R. Kitano, and R. Takai, *Lepton flavor physics at $\mu^+\mu^+$ colliders*, JHEP **06** (2023) 086, [[arXiv:2304.14020](#)].
- [38] **Muon g-2** Collaboration, B. Abi et al., *Measurement of the Positive Muon Anomalous Magnetic Moment to 0.46 ppm*,

- Phys. Rev. Lett. **126** (2021), no. 14 141801, [[arXiv:2104.03281](#)].
- [39] **Muon g-2** Collaboration, D. P. Aguillard et al., *Measurement of the Positive Muon Anomalous Magnetic Moment to 0.20 ppm*, Phys. Rev. Lett. **131** (2023), no. 16 161802, [[arXiv:2308.06230](#)].
- [40] **Muon g-2** Collaboration, D. P. Aguillard et al., *Measurement of the Positive Muon Anomalous Magnetic Moment to 127 ppb*, [arXiv:2506.03069](#).
- [41] R. Aliberti et al., *The anomalous magnetic moment of the muon in the Standard Model: an update*, [arXiv:2505.21476](#).
- [42] **BABAR** Collaboration, R. Godang, *Search for Muonic Dark Forces at BABAR*, EPJ Web Conf. **141** (2017) 02005, [[arXiv:1611.07934](#)].
- [43] R. Capdevilla, D. Curtin, Y. Kahn, and G. Krnjaic, *Systematically testing singlet models for $(g-2)_\mu$* , JHEP **04** (2022) 129, [[arXiv:2112.08377](#)].
- [44] **CMS** Collaboration, S. Chatrchyan et al., *Observation of Z Decays to Four Leptons with the CMS Detector at the LHC*, JHEP **12** (2012) 034, [[arXiv:1210.3844](#)].
- [45] W. Altmannshofer, S. Gori, M. Pospelov, and I. Yavin, *Neutrino Trident Production: A Powerful Probe of New Physics with Neutrino Beams*, Phys. Rev. Lett. **113** (2014) 091801, [[arXiv:1406.2332](#)].
- [46] **CMS** Collaboration, A. M. Sirunyan et al., *Search for an $L_\mu - L_\tau$ gauge boson using $Z \rightarrow 4\mu$ events in proton-proton collisions at $\sqrt{s} = 13$ TeV*, Phys. Lett. B **792** (2019) 345–368, [[arXiv:1808.03684](#)].
- [47] A. Kamada and H.-B. Yu, *Coherent Propagation of PeV Neutrinos and the Dip in the Neutrino Spectrum at IceCube*, Phys. Rev. D **92** (2015), no. 11 113004, [[arXiv:1504.00711](#)].
- [48] S. Gninenko and D. Gorbunov, *Refining constraints from Borexino measurements on a light Z' -boson coupled to L_μ - L_τ current*, Phys. Lett. B **823** (2021) 136739, [[arXiv:2007.16098](#)].
- [49] **NA64** Collaboration, Y. M. Andreev et al., *First Results in the Search for Dark Sectors at NA64 with the CERN SPS High Energy Muon Beam*, Phys. Rev. Lett. **132** (2024), no. 21 211803, [[arXiv:2401.01708](#)].
- [50] J.-Y. Cen, Y. Cheng, X.-G. He, and J. Sun, *Flavor specific $U(1)Bq-L_\mu$ gauge model for muon $g-2$ and $b \rightarrow s\mu^+\mu^-$ anomalies*, Nucl. Phys. B **978** (2022) 115762, [[arXiv:2104.05006](#)].
- [51] X. G. He, G. C. Joshi, H. Lew, and R. R. Volkas, *NEW Z-prime PHENOMENOLOGY*, Phys. Rev. D **43** (1991) 22–24.
- [52] R. Foot, X. G. He, H. Lew, and R. R. Volkas, *Model for a light Z-prime boson*, Phys. Rev. D **50** (1994) 4571–4580, [[hep-ph/9401250](#)].
- [53] Y. Cheng, X.-G. He, and J. Sun, *Widening the $U(1)L_\mu-L_\tau Z'$ mass range for resolving the muon $g-2$ anomaly*, Phys. Lett. B **827** (2022) 136989, [[arXiv:2112.09920](#)].
- [54] F. Huang and J. Sun, *Maximal flavor violating $U(1)L_\mu-L_\tau$ model with a singly charged scalar*, Phys. Rev. D **110** (2024), no. 11 115047, [[arXiv:2409.13249](#)].
- [55] X.-G. He, G. C. Joshi, H. Lew, and R. R. Volkas, *Simplest Z-prime model*, Phys. Rev. D **44** (1991) 2118–2132.
- [56] G. Lazarides, Q. Shafi, and C. Wetterich, *Proton Lifetime and Fermion Masses in an $SO(10)$ Model*, Nucl. Phys. B **181** (1981) 287–300.
- [57] R. N. Mohapatra and G. Senjanovic, *Neutrino Masses and Mixings in Gauge Models with Spontaneous Parity Violation*, Phys. Rev. D **23** (1981) 165.
- [58] W. Konetschny and W. Kummer, *Nonconservation of Total Lepton Number with Scalar Bosons*, Phys. Lett. B **70** (1977) 433–435.
- [59] T. P. Cheng and L.-F. Li, *Neutrino Masses, Mixings and Oscillations in $SU(2) \times U(1)$ Models of Electroweak Interactions*, Phys. Rev. D **22** (1980) 2860.
- [60] M. Magg and C. Wetterich, *Neutrino Mass Problem and Gauge Hierarchy*, Phys. Lett. B **94** (1980) 61–64.
- [61] J. Schechter and J. W. F. Valle, *Neutrino Masses in $SU(2) \times U(1)$ Theories*, Phys. Rev. D **22** (1980) 2227.
- [62] R. H. Parker, C. Yu, W. Zhong, B. Estey, and H. Müller, *Measurement of the fine-structure constant as a test of the Standard Model*, Science **360** (2018) 191, [[arXiv:1812.04130](#)].
- [63] A. Pich, I. Boyko, D. Dedovich, and I. I. Bigi, *Tau decays*, Int. J. Mod. Phys. A **24S1** (2009) 715–737.
- [64] **HFLAV** Collaboration, Y. S. Amhis et al., *Averages of b-hadron, c-hadron, and τ -lepton properties as of 2021*, Phys. Rev. D **107** (2023), no. 5 052008, [[arXiv:2206.07501](#)].
- [65] **Belle-II** Collaboration, L. Corona, *Tau and low multiplicity physics at Belle and Belle II*, [arXiv:2405.09974](#).
- [66] S. Ashanujjaman and K. Ghosh, *Revisiting type-II see-saw: present limits and future prospects at LHC*, JHEP **03** (2022) 195, [[arXiv:2108.10952](#)].
- [67] **CHARM-II** Collaboration, D. Geiregat et al., *First observation of neutrino trident production*, Phys. Lett. B **245** (1990) 271–275.
- [68] **CCFR** Collaboration, S. R. Mishra et al., *Neutrino Tridents and W Z Interference*, Phys. Rev. Lett. **66** (1991) 3117–3120.
- [69] **NuTeV** Collaboration, T. Adams et al., *Evidence for diffractive charm production in muon-neutrino Fe and anti-muon-neutrino Fe scattering at the Tevatron*, Phys. Rev. D **61** (2000) 092001, [[hep-ex/9909041](#)].
- [70] **Particle Data Group** Collaboration, S. Navas et al., *Review of particle physics*, Phys. Rev. D **110** (2024), no. 3 030001.
- [71] V. Shtabovenko, R. Mertig, and F. Orellana, *FeynCalc 10: Do multiloop integrals dream of computer codes?*, Comput. Phys. Commun. **306** (2025) 109357, [[arXiv:2312.14089](#)].
- [72] A. Alloul, N. D. Christensen, C. Degrande, C. Duhr, and B. Fuks, *FeynRules 2.0 - A complete toolbox for tree-level phenomenology*, Comput. Phys. Commun. **185** (2014) 2250–2300, [[arXiv:1310.1921](#)].
- [73] C. Degrande, C. Duhr, B. Fuks, D. Grellscheid, O. Mattelaer, and T. Reiter, *UFO - The Universal FeynRules Output*, Comput. Phys. Commun. **183** (2012) 1201–1214, [[arXiv:1108.2040](#)].
- [74] J. Alwall, M. Herquet, F. Maltoni, O. Mattelaer, and T. Stelzer, *MadGraph 5 : Going Beyond*, JHEP **06** (2011) 128,

- [arXiv:1106.0522].
- [75] T. Sjöstrand, S. Ask, J. R. Christiansen, R. Corke, N. Desai, P. Ilten, S. Mrenna, S. Prestel, C. O. Rasmussen, and P. Z. Skands, *An introduction to PYTHIA 8.2*, Comput. Phys. Commun. **191** (2015) 159–177, [arXiv:1410.3012].
- [76] **DELPHES 3** Collaboration, J. de Favereau, C. Delaere, P. Demin, A. Giammanco, V. Lemaitre, A. Mertens, and M. Selvaggi, *DELPHES 3, A modular framework for fast simulation of a generic collider experiment*, JHEP **02** (2014) 057, [arXiv:1307.6346].